IEEE Access
Multidisciplinary | Rapid Review | Open Access Journal

Date of publication xxxx 00, 0000, date of current version xxxx 00, 0000.

Digital Object Identifier 10.1109/ACCESS.2017.DOI

Progressive Semantic Face Deblurring

TAE BOK LEE[1], SOO HYUN JUNG[2], AND YONG SEOK HEO[1,2]
[1]Department of Artificial Intelligence, Ajou University, Worldcupro 206, Yeongtong-gu, Suwon 443-749, South Korea
[2]Department of Electrical and Computer Engineering, Ajou University, Worldcupro 206, Yeongtong-gu, Suwon 443-749, South Korea

Corresponding author: Yong Seok Heo (e-mail: ysheo@ajou.ac.kr).

This work was supported by the Ministry of Science and ICT (MSIT), South Korea, under the Information Technology Research Center (ITRC) Support Program supervised by the Institute for Information and Communications Technology Promotion (IITP) under Grant IITP-2020-2018-0-01424. The first two authors contributed equally to this work.

ABSTRACT Previous face deblurring methods have utilized semantic segmentation maps as prior knowledge. Most of these methods generated the segmentation map from a blurred facial image, and restore it using the map in a sequential manner. However, the accuracy of the segmentation affects the restoration performance. Generally, it is difficult to obtain an accurate segmentation map from a blurred image. Instead of sequential methods, we propose an efficient method that learns the flows of facial component restoration without performing segmentation. To this end, we propose a multi-semantic progressive learning (MSPL) framework that progressively restores the entire face image starting from the facial components such as the skin, followed by the hair, and the inner parts (eyes, nose, and mouth). Furthermore, we propose a discriminator that observes the reconstruction-flow of the generator. In addition, we present new test datasets to facilitate the comparison of face deblurring methods. Various experiments demonstrate that the proposed MSPL framework achieves higher performance in facial image deblurring compared to the existing methods, both qualitatively and quantitatively. Our code, trained model and data are available at https://github.com/dolphin0104/MSPL-GAN.

INDEX TERMS Facial image deblurring, semantic mask, progressive learning, generative adversarial network, deep learning

I. INTRODUCTION

FACIAL image deblurring is to restore a blurred face image as a sharp face image. Although human faces are highly variable, they have hierarchical structures that comprise components, such as skin, hair, eyes, nose, and mouth. These facial components are the crucial elements that characterize a specific face; each element has inherent shapes and textures. Thus, most face deblurring methods utilize the prior knowledge (i.e., reference face [1], [2], 3D face [3], face landmark [4], [5], 2D face sketch [6] and semantic segmentation map [7], [8]) of face images to estimate a unique solution.

Recently, deep learning-based methods [7], [8] have achieved state-of-the-art performances in facial image deblurring by utilizing the semantic segmentation map as prior knowledge. These methods consist of a two-step process that generates the segmentation map from the blurred image, and restores the facial image using this segmentation map in a sequential manner. In these methods, the semantic segmentation map is employed to localize the position of each facial component and the boundaries between them for the deblurring process.

However, these methods have a limitation. Accuracy of the estimated segmentation map affects the restoration performance due to their sequential properties. In general, it is nontrivial to obtain an accurate segmentation map from a blurred image. Inaccurate segmentation results often lead to inaccurate localization of facial components, and consequently generate a deblurred result with distorted shapes and/or blurred textures [3], [9].

Specifically, small components of the face (that is, the eyebrows, eyes, nose, and lips) which characterize the faces, are significantly affected by inaccurate segmentation compared to the large components such as hair and skin. In general, each facial component is different in size, and has large deviations. For instance, the eyes have a very small number of pixels compared to the skin or hair regions. Moreover, these small components of the face are more likely to lose information due to noise and blur artifacts than the large components. Due to this degradation, it is difficult to obtain accurate semantic segmentation maps especially for small components from the blurred images. Thus, small components require more attention than the large components for the restoration of their exact shapes and textures. This problem, called the

This article has been accepted for publication in a future issue of this journal, but has not been fully edited. Content may change prior to final publication. Citation information: DOI 10.1109/ACCESS.2020.3033890, IEEE Access

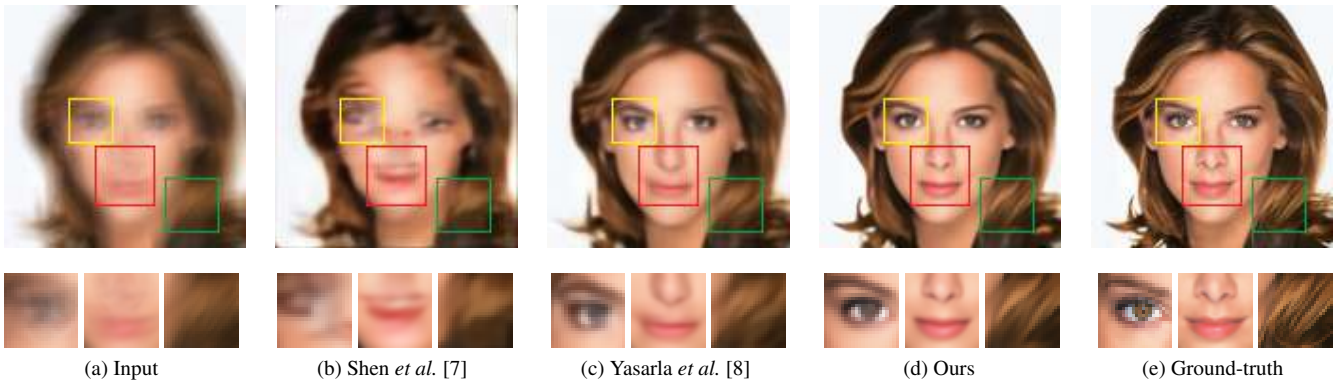

(a) Input (b) Shen *et al.* [7] (c) Yasarla *et al.* [8] (d) Ours (e) Ground-truth

FIGURE 1. Qualitative comparison of the proposed method and existing face deblurring methods. Our approach reconstructs more textures and finer details of facial components such as the eyes, nose, mouth, and hair.

class imbalance in Yasarla *et al.* [8], is one of the major challenges in the previous method [7], [8].

As investigated in [3], [8], Shen *et al.* [7] often fails to restore the small components of the face when the generated segmentation results are inaccurate. To address this problem, Yasarla *et al.* [8] proposed measuring the confidence score of the facial components from the generated segmentation. If the estimated segmentation maps have low confidence, their model reduces the impact of segmentation maps in the deblurring process. This method can effectively reduce the effects of inaccurate segmentation maps. However, their solution is suboptimal, because they do not provide how to utilize the semantic prior when the segmentation map is inaccurate due to severe blurs.

To deal with this problem, we propose a multi-semantic progressive learning (MSPL) framework based on the generative adversarial network (GAN) [10]. Our method leverages the semantic prior information of the face without performing segmentation to prevent the side effects of an inaccurate segmentation map. Furthermore, our method progressively restores the face within four steps, inspired by the success of progressive learning techniques [11], [12]. Conventional progressive learning [11], [12] does not consider the semantic context of the target object in an image. Therefore, we modified the concept of the conventional coarse-to-fine approach to understand the underlying semantic structure of the target object better.

Specifically, the proposed generator network has a cascaded architecture with sub-networks to restore the entire face progressively and incrementally, starting with the simpler facial components. Our network is trained to focus on low-frequency components first and then incrementally restore the smaller and high-frequency components in the face image, instead of learning all the components of the face image simultaneously. During training, each sub-network focuses on restoring both the shape and texture for their assigned class-specific facial components. This is achieved by minimizing the difference between the sharp and output facial components using masks obtained by precise ground-truth segmentation maps. In addition, the architecture of our generator mitigates the class-imbalance problem. The proposed generator consists of multiple sub-networks. Each sub-network is trained to focus on restoring the assigned facial key component. This simple method allows the proposed method to handle the class imbalance problem of face deblurring more effectively. Fig. 1 clearly shows the effects of the proposed framework. Our MPSL framework restores a sharper face with fine-detailed facial components compared to the previous methods [7], [8].

To generate facial images that are more photo-realistic, we propose a multi-semantic discriminator in our GAN framework. It is designed to handle all the intermediate outputs of the generator using a single classifier network by allowing the flow of gradients at all semantic components in the discriminator to the generator. Through this, our discriminator oversees the entire flow of reconstructions of the facial components.

To the best of our knowledge, there are only a few public test datasets avaliable for facial image deblurring. Shen *et al.* [7] provided a pioneering test dataset for evaluation. However, most of the provided images are of low quality with unknown blocking artifacts. In addition, all of the test faces are well aligned and centered with the same facial key points. However, in the real-world scenarios, faces are captured in various shapes and poses. Thus, these images are not appropriate to fully evaluate various methods for a range of cases; in view of this, we provide new test datasets that are suitable for a more practical evaluation of face deblurring.

The contributions of our work are summarized as follows:

- We propose an MSPL network, which progressively learns the semantics of a human face for deblurring the facial images from complex motion blur. To the best of our knowledge, this is the first time that the idea of a semantic coarse-to-fine manner has been introduced in face deblurring.
- We propose the Multi-Semantic discriminator, which can observe all the outputs of a generator. From this, our generator reconstructs more photo-realistic face compo-

nents in addition to the entire face.
- To conduct a more accurate and practical evaluation of face deblurring, we suggest new test datasets with extensive and high-quality images. The experimental results show that the proposed model significantly outperforms the previous methods.

The remainder of this paper is organized as follows. Section II provides an overview of the previous works on image deblurring. In Section III, we present the details of our proposed framework. Section IV provides the quantitative and qualitative results of the proposed method compared to the existing methods. Finally, Section V presents the conclusions and discusses the future works.

II. RELATED WORK

Image deblurring has been studied for a long time in the field of image processing and computer vision. In this section, we briefly review the image deblurring methods and recent deep learning-based progressive learning approaches.

A. GENERIC IMAGE DEBLURRING

Single image deblurring is a highly ill-posed problem; thus, the traditional deblurring methods utilize natural image priors, such as sparsity priors [13], [14], L_0 gradient priors [15], low-rank priors [16], patch priors [17], [18] and channel priors [19], [20]. Although these handcrafted priors suffice for a small subset of the scene, it is difficult to apply them to real-world images with complex blurs.

After the advent of deep learning [21], various convolutional neural network (CNN) models have been proposed to estimate the complex blur kernels [22], [23]. Sun *et al.* [22] proposed to predict the probabilistic distribution of motion blur at patch level. Chakrabarti *et al.* [23] predicted the complex Fourier coefficients of a deconvolution filter and applied them to an input patch. These methods combine the CNNs and maximum a posteriori probability (MAP)-based algorithms. On the other hand, several CNN models directly restore the sharp image from blurred image in an end-to-end manner [24]–[29]. Nah *et al.* [24] proposed a multi-scale CNN model. They first extended the traditional coarse-to-fine pipeline to a CNN-based deblurring field and achieved impressive results. Tao *et al.* [25] investigated a multi-scale strategy for the recurrent neural network (RNN) based multi-scale architecture. To restore the realistic images, Kupyn *et al.* [30] introduced a GAN-based deblurring model that exploited Wasserstein GAN with a gradient penalty and perceptual loss.

B. FACE IMAGE DEBLURRING

While the aforementioned methods perform well for natural image deblurring, they often do not perform satisfactorily on domain-specific images such as face images. Therefore, several studies have proposed estimating various types of prior facial knowledge such as the face alignment [4], face sketches [6], reference faces [2], [31], 3D face models [3], and face segmentation maps [7], [8]. The reference prior-based methods [2], [31] extract useful information to restore the face image from a sharp face similar to a degraded face image. However these methods require a redundant collecting and matching computation process to utilize the exemplar face images. Ren *et al.* [3] proposed a video deblurring method for faces by generating 3D facial priors. They trained the 3D face reconstruction network to estimate more textured facial priors. Despite satisfactory result on video deblurring, their model was unable to perform on a single image. More recently, Shen *et al.* [7] and Yasarla *et al.* [8] proposed the use of semantic prior of the face for the deblurring process and achieved state-of-the-art results. These methods are two-step process. The steps include generating the semantic labels from the blurred face first, and then using them as strong prior knowledge for the deblurring process. However, extracting the segmentation map from the blurred face is difficult, and the erroneous prior information directly degrades the quality of the reconstructed face image. To reduce the side effects of inaccurate segmentation maps, Yasarla *et al.* [8] proposed measuring the confidence score of an estimated semantic map. However, they do not provide how to utilize the semantic prior when the segmentation map is inaccurate due to severe blurs. Unlike previous works [7], [8], the proposed method exploits only the ground-truth segmentation maps for training purposes, instead of generating them from blurred images. Using this procedure, our method can be trained with accurate segmentation maps, regardless of the degree of blurs, and prevent the side effects of inaccurate segmentation maps. In addition, the architecture of the proposed generator allows the restoration of the small components of the face more effectively.

C. PROGRESSIVE LEARNING

Progressive learning is a training strategy that involves starting with an easy task and gradually refining the details. Most existing methods that use progressive learning are based on a multi-scale (coarse-to-fine) approach. Multi-scale frameworks have made significant progress in estimating complex motion blur kernels in single image deblurring [13], [24], [25], [32], [33]. In addition to the single image deblurring field, the multi-scale approach is widely used in other image processing fields such as depth map estimation [34]–[36], and video frame prediction [37]. In recent years, progressive learning [11], [12], [20], [38]–[42] has been actively applied to CNN-based image synthesis. In particular, Karras *et al.* [11] proposed a progressive growing technique that progressively increases the depth of the layer as well as the resolution of the generated image. Karnewar *et al.* [12] proposed the multi-scale gradient generative adversarial network (MSG-GAN) by allowing the flow of gradients from the discriminator to the generator at multi-scales. Meanwhile, Yang *et al.* [43] proposed a method to generate the background and foreground recursively and separately. In contrast to the conventional methods, we suggest progressive learning techniques according to the semantic information of the face.

This article has been accepted for publication in a future issue of this journal, but has not been fully edited. Content may change prior to final publication. Citation information: DOI 10.1109/ACCESS.2020.3033890, IEEE Access

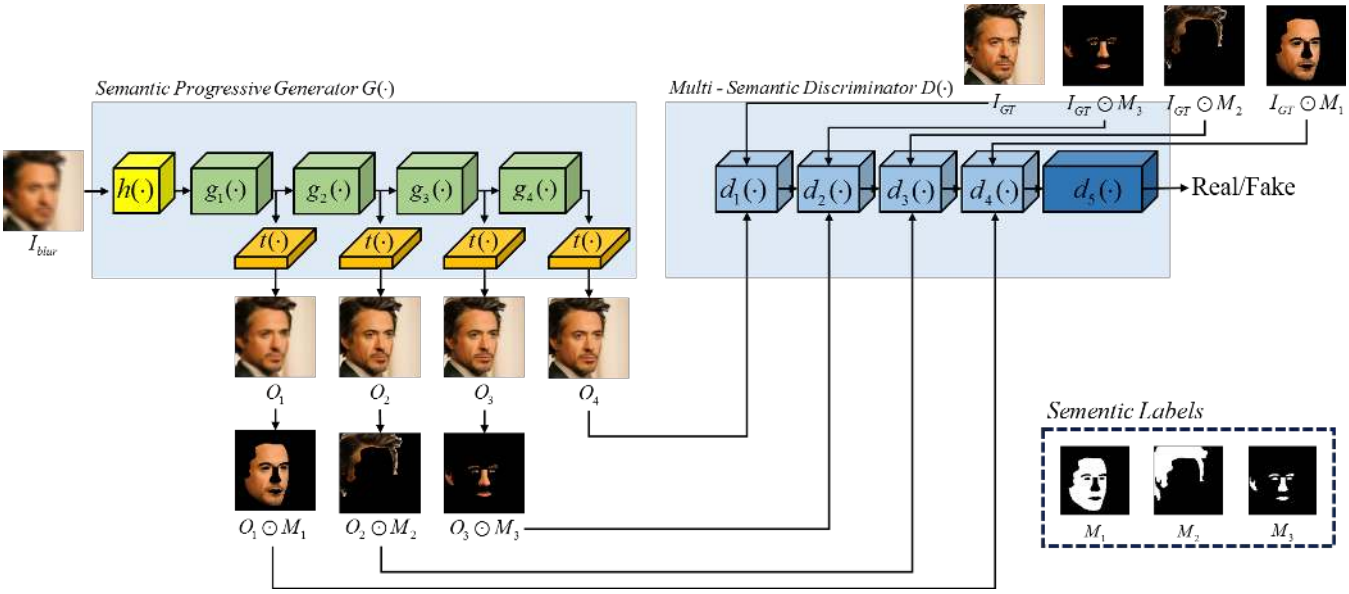

FIGURE 2. Overview of the proposed face deblurring framework comprising of a generator and a discriminator. The generator reconstructs the image in four steps, and the discriminator observes all the output images from the generator.

III. PROPOSED METHOD

As illustrated in Fig. 2, our MSPL framework is composed of a generator (G) and a discriminator (D). G generates a sharp face image I_{deblur} from a blurred face image I_{blur}. Our proposed G incrementally generates the facial components step-by-step in the order of skin, hair, inner parts (eyes, nose, and mouth), and then the entire face. Meanwhile, the proposed discriminator (D) oversees all the generated face image components from the G. A detailed explanation of each network is provided in the following subsections.

A. SEMANTIC PROGRESSIVE GENERATOR

Following Yasarla *et al.* [8], we divide the ground-truth segmentation labels into three classes as follows: $M_1 = \{skin\}$, $M_2 = \{hair\}$, $M_3 = \{nose, eyes, eyebrows, ears, mouth, lip\}$, and $M_4 = \{entire\}$. Here, M_i is a binary mask image with 1 for the assigned region, and 0 for other regions. Note that M_4 represents the entire area of the image, including the face and background. From Fig. 2, it can be observed that G consists of multiple functional blocks as h, g_i, and t, where $1 \leq i \leq 4$. First, h is an initial 1×1 convolution layer that converts an input RGB image I_{blur}, to a feature map F_{init}, for the following layer g_1. Thus, h can be defined as $h : I_{blur} \mapsto F_{init}$. Second, g_i is a function of our sub-network defined by

$$g_i : F_{i-1} \mapsto F_i \,, \; where \; 1 \leq i \leq 4, \; F_0 = F_{init}. \quad (1)$$

Finally, t is a 1×1 convolution layer that converts the output feature map F_i generated from g_i to an output RGB image O_i, as $t : F_i \mapsto O_i$. Then, the O_i can be defined as

$$O_i = t(g_i(F_{i-1})) = t(F_i), \; where \; 1 \leq i \leq 4. \quad (2)$$

Thus, the entire network G can be defined as a sequential composition of all sub-networks as

$$G : I_{blur} \mapsto \{O_1, O_2, O_3, O_4\}. \quad (3)$$

In our framework, g_i is the key module of our network that focuses on restoring each semantic structure of the face. Each g_i shares the same network architectures; however, their roles are different as each g_i renders each facial component using the previous feature maps generated from the g_{i-1} layer. For this, we design each g_i as a fully convolutional U-shaped network, which consists of residual blocks [44]. As investigated in [45], [46], we remove the normalization layers from the standard residual blocks because the normalization layers get rid of flexibility from the network for low-level tasks. To extract more focused features, we apply a channel-attention mechanism [47], [48] to our residual blocks. The entire architecture of g_i is shown in Table 1. In Table 1, each row of the "Kernel" column specifies the kernel size and, the number of filters and strides. For example, "3×3, 64, s1" represents the 64 filters of size 3×3, with stride 1.

Our goal is to train each g_i to reconstruct the assigned facial component perfectly. For this, we define the facial component loss ($\mathcal{L}_i^c$), which is defined as L_1 distance between the facial components of the ground truth (GT) images and those generated from g_i as

$$\mathcal{L}_i^c = \left\| (I_{GT} \odot M_i) - (O_i \odot M_i) \right\|_1, \quad (4)$$

where $\odot$ represents the Hadamard product. To refine the entire face more naturally and restore the background of the face, we compare the last output image O_4, and the entire target image I_{GT}. This allows all sub-networks to share a common objective and provide stability during training. The

This article has been accepted for publication in a future issue of this journal, but has not been fully edited. Content may change prior to final publication. Citation information: DOI 10.1109/ACCESS.2020.3033890, IEEE Access

TABLE 1. Architecture of the proposed sub-network (g_i). F_{i-1} is an input feature of i^{th} sub-network g_i. "W" and "H" represent the width and height of the feature, all of the "downconv" layers represent convolutional layer with stride 2 for the downsampling operation, and "upconv" layers represent the transpose convolution for upsampling, and "+" represents a channel-wise sum operation.

Blocks	In→Out	Kernel	Output size
Resblock×2	F_{i-1} →r1	3×3, 128, s1	W×H
downconv1	r1→d1	4×4, 128 s2	(W/2)×(H/2)
Resblock×2	d1→r2	3×3, 128, s1	(W/2)×(H/2)
downconv2	r2→d2	4×4, 128, s2	(W/4)×(H/4)
Resblock×4	d2→r3	3×3, 128, s1	(W/4)×(H/4)
upconv1	r3→u1	4×4, 128, s2	(W/2)×(H/2)
Resblock×2	r2+u1→r3	3×3, 128, s1	(W/2)×(H/2)
upconv2	r3→u2	4×4, 128, s2	W×H
Resblock×2	r1+u2→ F_i	3×3, 128, s1	W×H

TABLE 2. Architecture of the proposed discriminator. All the multiple input images are denoted as x_1, x_2, x_3 and x_4. "lReLU" is a leaky ReLU, "SN" is a spectral normalization, and "$\oplus$" represents a channel-wise concatenation operation.

Blocks	Operation	In→Out	Kernel
d_1	Conv2d, lReLU, SN	$x_1 \rightarrow A_1$	3×3, 64, s1
d_2	Conv2d, lReLU, SN	$x_2 \rightarrow$C2	3×3, 64, s1
	Conv2d, lReLU, SN	C2$\oplus A_1 \rightarrow A_2$	3×3, 64, s1
d_3	Conv2d, lReLU, SN	$x_3 \rightarrow$C3	3×3, 64, s1
	Conv2d, lReLU, SN	C3$\oplus A_2 \rightarrow A_3$	3×3, 64, s1
d_4	Conv2d, lReLU, SN	$x_4 \rightarrow$C4	3×3, 64, s1
	Conv2d, lReLU, SN	C4$\oplus A_3 \rightarrow A_4$	3×3, 64, s1
d_5	Conv2d, lReLU, SN	$A_4 \rightarrow$C5	4×4, 64, s2
	Conv2d, lReLU, SN	C5→C6	4×4, 128. s2
	Conv2d, lReLU, SN	C6→C7	4×4, 256, s2
	Conv2d, lReLU, SN	C7→C8	4×4, 512, s2
	Conv2d, lReLU, SN	C8→p	4×4, 1, s2

total facial component loss of our G ($\mathcal{L}_G$) can be formulated as follows:

$$\mathcal{L}_G = \sum_{i=1}^{4} \mathcal{L}_i^c. \tag{5}$$

Our proposed objective function in Eq. (5) allows a single g_i to focus on the specified facial component using only ground-truth segmentation maps. Thus, our G is able to reconstruct more precise shapes and finer details of the target face without suffering from the side effects of using an inaccurate segmentation map.

B. MULTI-SEMANTIC DISCRIMINATOR

We also propose a multi-semantic discriminator D in our method. Inspired by the MSG-GAN [12], our D handles multiple outputs of G which allows the restoration of more realistic facial components at all intermediate layers. As shown in Fig. 2, multiple intermediate images are fed to our single D. Thus, a single network D is a function of multiple input images and predicts a final probability $p \in [0, 1]$ as

$$D : \{x_1, x_2, x_3, x_4\} \mapsto p, \tag{6}$$

where x_j is a j^{th} input RGB image of D. Let d_j be the j^{th} intermediate layer of D, and let A_j be an output feature map of d_j. Then, d_j can be defined as

$$d_j : (x_j, A_{j-1}) \mapsto A_j, \; where \, 1 \leq j \leq 4, \; A_0 = \emptyset. \tag{7}$$

Each d_j consists of a 3×3 convolutional layer c, and a single concatenation operation. Then, A_j is formulated as

$$A_j = d_j(x_j, A_{j-1}) = c(c(x_j) \oplus A_{j-1}), \tag{8}$$

where $\oplus$ represents a channel-wise concatenation operation. D is alternatively trained using either the ground-truth image or the result of G. Thus, when training D with the outputs from G, x_1 becomes O_4, and x_j is the generated facial component ($O_{5-j} \odot M_{5-j}$), where $2 \leq j \leq 4$. On the other hand, when x_j is the ground-truth facial component ($I_{GT} \odot M_{5-j}$), D learns the real face component, and x_1 is I_{GT}. Then, the last block d_5 acts as a classifier to estimate the probability of multiple input images being real or fake. Table 2 shows the detailed architecture of our discriminator. We applied spectral normalization [49] to all the convolutional layers to stabilize the training of discriminator.

Following Goodfellow et al. [10], we optimized G and D in an alternating manner to solve the following adversarial min-max function $V(G, D)$:

$$\min_G \max_D V(D, G) = \\ \mathbb{E}_y[\log D(y)] + \mathbb{E}_{I_{blur}}[\log(1 - D(G(I_{blur})))]. \tag{9}$$

Here, y is a set of images corresponding to the ground-truth components of faces as $y = \{y_i | y_i = (I_{GT} \odot M_i), \, 1 \leq i \leq 3, \, y_4 = I_{GT}\}$. Then, the adversarial loss ($\mathcal{L}_{adv}$) is defined as follows:

$$\mathcal{L}_{adv} = -\log(D(G(I_{blur}))). \tag{10}$$

During training the generator, the error is backward-propagated to the intermediate layers of G from the intermediate layers of the D simultaneously. This provides stability in training, because the sub-networks of the generator can share the same goal. Meanwhile, the discriminator observes not only the final output of G, but also all the intermediate outputs of G.

Recently, perceptual loss [50] has been widely adopted for better visual quality. To take advantage of this, we employed a VGG-face loss $\mathcal{L}_{vgg}$ which is defined by

$$\mathcal{L}_{vgg} = \left\| \phi(I_{GT}) - \phi(I_{deblur}) \right\|_1, \tag{11}$$

where $\phi(\cdot)$ represents the feature extracted from the $Pool5$ layer of the VGG-Face network [51].

The total loss of our MSPL framework $\mathcal{L}_{total}$ is the combination of all the above loss functions discussed so far ($\mathcal{L}_G$ in Eq. (5), $\mathcal{L}_{adv}$ in Eq. (10), and $\mathcal{L}_{vgg}$ in Eq. (11)) as

$$\mathcal{L}_{total} = \mathcal{L}_G + \lambda_1 \mathcal{L}_{adv} + \lambda_2 \mathcal{L}_{vgg}, \tag{12}$$

where λ_1 and λ_2 represent the weights used to balance the different loss terms. We empirically set the weights of our loss terms as $\lambda_1 = 0.05$ and $\lambda_2 = 0.05$.

This article has been accepted for publication in a future issue of this journal, but has not been fully edited. Content may change prior to final publication. Citation information: DOI 10.1109/ACCESS.2020.3033890, IEEE Access

(a) Shen *et al.* [7] (b) MSPL-Center (c) MSPL-Random

FIGURE 3. Comparison of testsets of Shen *et al.* [7] and our MSPL testsets. The sample ground-truth faces from (a) Shen *et al.* [7], (b) MSPL-Center, and (c) MSPL-Random testset.

TABLE 3. Results of image quality assessment on face deblurring testsets. We compare the quality of GT images using the four image quality assessment metrics. Each result is an average of the number of GT images. Best results are highlighted as bold.

Testset	# GT images	NIQE [52] (↓)	BRISQUE [53] (↓)	NRQM [54] (↑)	PIQE [55] (↓)	PI [56] (↓)
Shen *et al.* [7] Testset	200	18.8742	34.5743	5.8856	48.2324	11.4944
MSPL-Center	240	**18.8740**	**30.3057**	**6.6018**	**42.5591**	**11.1363**

TABLE 4. Results of image quality assessment on CelebA images in testsets. Best results are highlighted in bold.

CelebA	# GT images	NIQE [52] (↓)	BRISQUE [53] (↓)	NRQM [54] (↑)	PIQE [55] (↓)	PI [56] (↓)
Shen *et al.* [7] Testset	100	18.8744	32.7266	6.0758	43.6343	11.3992
MSPL-Center	80	**18.8743**	**30.7639**	**6.6247**	**42.6092**	**11.1265**

IV. EXPERIMENTAL RESULTS

A. DATASETS

1) Training Data

For training, we used the CelebAMask-HQ dataset [57], which provides 30,000 high-quality (1024×1024 resolution) face images. Each image has 19 classes of segmentation labels such as skin, nose, eyes, eyebrows, ears, mouth, lips, hair, hat, eyeglass, earring, necklace, neck, and cloth. We regrouped these labels into three classes, which are the skin, hair and inner parts, as [8]. Following [58], we synthesized 18,000 motion blur kernels using the method of [23]. As trained in [7], [58], the size of the generated motion blur kernels ranges from 13×13 to 27×27. After applying the blur kernel to the image, we added Gaussian noise with $\sigma = 0.03$. The generated images were then split into two subsets: the training images (24,183 images), and the validation images (5,817 images).

2) Test Data

For face deblurring, Shen *et al.* [7] provide a pioneering testset to evaluate the motion-blurred faces. However, many GT images in the testset are of low quality with unknown block artifacts (see Fig. 3(a)). Because the purpose of image deblurring is to restore a sharp and high-quality image, these low-quality GT images are not suitable for evaluating performance. In addition, facial images in their testset are well aligned with the same facial key points [59]. However, the blurred face images are not aligned in the real world, because faces are usually captured under a wide range of conditions. Therefore, their testset does not condsider the practical situations where these blurred face images occur. Therefore, we generated two types of test datasets called the MSPL-Center and MSPL-Random. We collected 240 sharp face images from three different datasets (i.e., 80 images each from CelebA [60], CelebAMASK-HQ (CelebA-HQ) [57] and Flickr-Faces-HQ thumbnails (FFHQ) [42]). Note that each dataset is aligned with different facial key points. Subsequently, we synthesized 240 random motion blur kernels using the method presented in [23]. Following the protocol by Shen *et al.* [7], the size of blur kernels ranges from 13×13 to 27×27. As shown in Fig. 3(b), MSPL-Center contains high-quality and differently aligned face images. Meanwhile, MSPL-Random comprises images that are randomly augmented versions using MSPL-Center (samples are shown in Fig. 3(c)). To be specific, we conducted random crops, random rotation, and random horizontal flips to the MSPL-Center images and convolved the random blur kernels synthesized using [23].

This article has been accepted for publication in a future issue of this journal, but has not been fully edited. Content may change prior to final publication. Citation information: DOI 10.1109/ACCESS.2020.3033890, IEEE Access

3) Image Quality Comparison

Following [61]–[63], we used four of the no-reference image quality assessment (NRIQA) metrics (i.e., NIQE [52], BRISQUE [53], NRQM [54], and PIQE [55]) to compare the quality of the images of our testset (MSPL-Center) and testset provided by Shen *et al.* [7]. The NIQE and BRISQUE metrics measure the image naturalness (or its lack thereof) based on their own natural scene statics (NSS) model [52], [53]. NRQM provides the quality scores of the images based on extracted features from the trained CNN model [54]. PIQE is a perception-based image quality evaluation method that estimates the amount of distortion present in a given image [55]. We also employ the perception index (PI) metric [56], which is formulated as the adjusted mean value of NIQE and NRQM.

Shen *et al.* [7] and MSPL-Center testsets were compared because they both consist of centered facial images. As aforementioned, the face images in MSPL-Random are randomly transformed version of the MSPL-Center. Thus, we do not compare the MSPL-Random dataset with the Shen *et al.* [7] testset. All the results of image assessments are listed in Table 3. When comparing [7] and MSPL-Center, the values of NIQE are comparable. However, the MSPL-Center dataset achieved better BRISQUE, NRQM, and PIQE than the Shen *et al.* [7] testset.

For a fair comparison, we evaluated the image quality of the Shen *et al.* [7] and MSPL-Center subsets, both of which were synthesized using CelebA [60]. The results in Table 4 show that the test images in Shen *et al.* [7] are clearly degraded compared to those in MSPL-Center, even when considering the images selected from the same face dataset [60]. These assessment metrics quantify the noise, artifacts, sharpness and overall quality of the image. Therefore, the comparative results indicate that the Shen *et al.* [7] testset consist of low-quality GT images and the proposed MSPL testsets are more suitable for the evaluation of face deblurring performance.

B. TRAINING DETAILS

To implement our models, we used Pytorch [64]. The generator and discriminator were trained using the Adam optimizer [65] with $\beta_1 = 0.9$, $\beta_2 = 0.999$. The learning rate was initialized as 1×10^{-5} and decayed exponentially by a factor of 0.99 for every epoch. When training, we first resized the 1024×1024 images to 512×512 images using bilinear downsampling. Then, we randomly cropped the images to 448×448 and resized them to 128×128. We augment the resized images with random horizontal flips and random rotations in the range [0°, 90°]. We set the batch size as 16 and trained the model with a single NVIDIA TITAN-RTX GPU.

C. EVALUATION METRICS

To evaluate the performances of various methods, we used PSNR and SSIM [66], which are widely used in image restoration fields. The feature distance (d_{VGG}) of the VGG-Face network [67] was measured to compare the similarity in facial identity between the GT images and the deblurred face images. Following [68], we computed the L_2 distance using the output features from the $Pool5$ layer of the VGG-Face network [67]. Following the 2020 NTIRE challenge [63], we employed the LPIPS [69] distance, which is computed as the L_2 distance using the output features from the learned CNN for computing human visual perception.

TABLE 5. Ablation studies on CelebA of MSPL-Center Testset. All inner components of the face is denoted as "Inner", and the whole image as "Entire". Best result is highlighted as bold.

Method	Intermediate outputs of G (corresponding mask)				PSNR	SSIM
	O_1	O_2	O_3	O_4		
Baseline	-	-	-	Entire (M_4)	28.12	0.922
MSPL_a	Entire (M_4)	Skin (M_1)	Hair (M_2)	Inner (M_3)	27.17	0.906
MSPL_b	Inner (M_3)	Hair (M_2)	Skin (M_1)	Entire (M_4)	28.00	0.920
MSPL w/o GAN	Skin (M_1)	Hair (M_2)	Inner (M_3)	Entire (M_4)	**28.67**	**0.923**
MSPL_GAN	Skin (M_1)	Hair (M_2)	Inner (M_3)	Entire (M_4)	28.07	0.921

TABLE 6. PSNR values for each facial component on CelebA-HQ in MSPL-Center Testset. We measured the metrics using individual classes of GT segmentation maps.

Method	Facial Components			
	Skin	Hair	Inner parts	Average
	PSNR(↑)	PSNR(↑)	PSNR(↑)	PSNR(↑)
Shen *et al.* [7]	19.75	19.76	16.16	18.56
Yasarla *et al.* [8]	23.52	22.55	19.46	21.85
MSPL w/o GAN O_1	26.77	24.40	19.10	23.42
MSPL w/o GAN O_2	27.30	26.58	22.68	25.52
MSPL w/o GAN O_3	28.30	27.22	24.84	26.79
MSPL w/o GAN O_4	**30.40**	**28.31**	**25.74**	**28.15**

D. ABLATION STUDY

1) Effect of the Semantic Progressive Generator

To investigate the impacts of the reconstruction procedure of the face components, we gradually modified the baseline model and compared the differences. We set the baseline model to the same architecture as G, with the difference being that it is trained without facial component losses ($\mathcal{L}_1^c$, $\mathcal{L}_2^c$, and $\mathcal{L}_3^c$) and discriminator. Thus, the baseline model generates only a single output image at the final image convert layer ($t(F_4)$) of G. This baseline was trained with only $\mathcal{L}_4^c$ loss between the O_4 and I_{GT}, which is commonly used in image restoration studies. From this baseline model, we added intermediate output layers and compared the performance of the models (denoted as MSPL) trained with different restoration procedures.

Table 5 shows the performances of all the conducted models trained with different reconstruction procedures and identical training settings and data. The M_i specified in Table 5 represents the semantic mask used to train the corresponding intermediate output of the MSPL model. MSPL_a is a model that is trained to restore a blurry input image in the order of entire image, skin, hair, and inner components. Comparing the results of MSPL_a and other models, it can be observed that restoring the entire face from the last module is crucial to the accuracy of the restoration process. MSPL_b is a trained

This article has been accepted for publication in a future issue of this journal, but has not been fully edited. Content may change prior to final publication. Citation information: DOI 10.1109/ACCESS.2020.3033890, IEEE Access

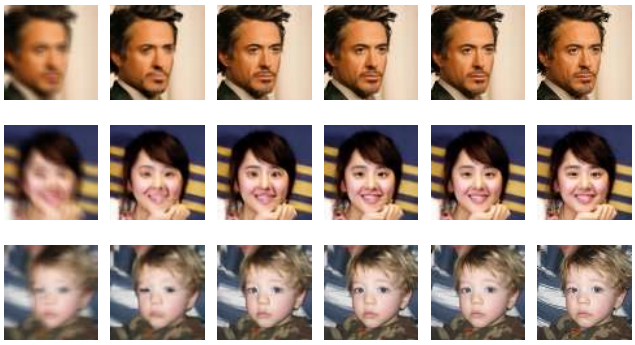

(a) Input (b) O_1 (c) O_2 (d) O_3 (e) O_4 (f) GT

FIGURE 4. Intermediate outputs of the proposed network.

model in reverse order of the proposed method except the entire component. This model restores the facial components starting from small and high-frequency components first (inner components), and restore the large and low-frequency components (hair, skin) later. The results of the MSPL_b also show that the wrong order of the face reconstruction degrades the deblurring performance. MSPL w/o GAN is a model trained to restore facial components with the proposed procedure using Eq. (5). The results in Table 5 demonstrate that the architecture trained with the proposed order improves the restoration performance compared to the other orders.

In addition, Table 6 quantitatively demonstrates the effect of our progressive generator for each facial component. When comparing the PSNRs of O_1, O_2, O_3, and O_4, we can confirm that the PSNR values of all the facial components gradually increase. These results indicate that the proposed method performs the deblurring incrementally. All the sub-networks enhance the quality of the image compared to the output image of the previous stage. Furthermore, we can observe that each sub-network is gradually improving not only the class-specific component, but also the entire face. This is because all the sub-networks share the goal of restoring the whole face. This lends stability to our progressive training method.

In Fig. 4, we can qualitatively observe the deblurring procedure in our proposed method that progressively restores the face image in the order of skin, hair, inner parts (eyes, eyebrows, nose, and mouth) and the entire face. From a blurred input face, the first sub-network generates the first output image O_1. At this stage, we can see that the overall shape of the facial skin is restored excluding the other facial components (see Fig. 4(b)). In Fig. 4(c), we confirm that the shape and texture of the hair in O_2 are restored from O_1. However, some blurred artifacts remain in the facial inner parts and background. In the third stage, the O_3 (Fig. 4(d)) shows that the inner parts of the face are significantly restored compared to O_2 from the previous stage. The final output image O_4 is shown in Fig. 4(e). The final result demonstrates that the final sub-network recovers the entire face and background. In particular, the facial components of O_4 are more natural compared to those of O_3.

2) Effect of the Multi-Semantic Discriminator

In our MSPL framework, the multi-semantic discriminator is utilized to recover the faces that are more photo-realistic. To study the effects of this, we additionally trained our generator model with the proposed discriminator and trained with $\mathcal{L}_{total}$ in Eq. (12). We denote our model as MSPL_GAN which are trained with the loss function $\mathcal{L}_{total}$ in Eq. (12). The results listed in Table 5 indicate that the MSPL_GAN achieves slightly poor results compared to those archived by MSPL w/o GAN. However, the visual results presented in Fig. 5 show that our discriminator assists in reconstructing the faces that are more realistic. In Fig. 5, we compare the results of MSPL w/o GAN and MSPL_GAN (the odd rows and the even rows in Fig. 5, respectively) with the same blurred image as the input. It can be observed that the MSPL_GAN model restores the more realistic facial components than those restored by the MSPL w/o GAN model, especially for the nose, mouth, eyes, and texture of hair. For example, the output images in the second row contain more a realistic nose and mouth than the outputs in the first row. When comparing the images in the third and fourth rows, we can see a clear effect of GAN. This demonstrates the effect of our multi-semantic discriminator that allows the generator to restore the more realistic facial components. In addition, we confirm that our discriminator can affect on not only the final output image O_4, but also all the intermediate outputs from O_1 to O_3. In our experiments, the performance of MSPL_GAN model was slightly lower in the PSNR/SSIM compared to those of the MSPL w/o GAN model. However, MSPL_GAN model can restore the more visually plausible outputs that contain inner components, which are more natural, by using our multi-semantic discriminator.

E. COMPARISONS WITH EXISTING METHODS

We compared the performance of our MSPL framework with recent methods based on CNN models [7], [8], [58], [68], [70]. All the experiments were conducted using the official codes provided by the authors [7], [8], [58], [68], [70]. For Xia and Chakrabarti [58], we used the model trained in a supervised manner, as this model has been reported as the best model in their studies. Since Zhang *et al.* [70] was originally trained on the natural scene images, we retrain their model using our training data to compare under fair condition, which is denoted as *Zhang *et al.* [70].

1) Class Imbalance Problem

As mentioned earlier, the class imbalance problem is an important and challenging issue for the existing face deblurring methods [7], [8]. To compare the restoring capability of restoring the small and thin components of the face (such as the eyes, lips, and eyebrows), we compared the PSNR value of each individual class in the face using a ground-truth segmentation map, following the experiment presented by Yasarla *et al.* [8].

This article has been accepted for publication in a future issue of this journal, but has not been fully edited. Content may change prior to final publication. Citation information: DOI 10.1109/ACCESS.2020.3033890, IEEE Access

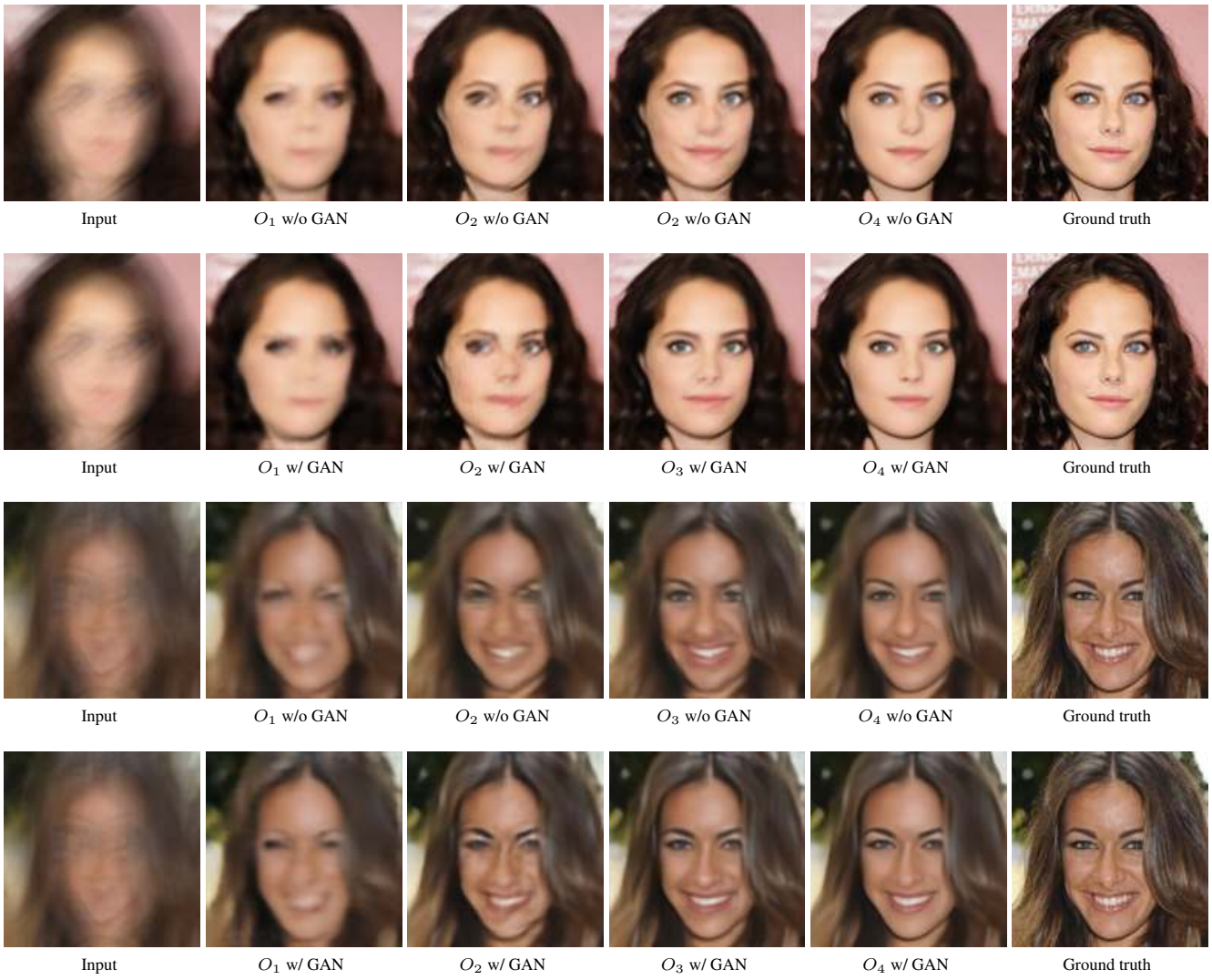

FIGURE 5. Comparisons of MSPL w/o GAN and MSPL_GAN. From left to right, input blurred faces, O_1, O_2, O_3, O_4, and the GT faces; rows 1 and 3 of the figure are the results of the MSPL w/o GAN, rows 2, and 4 are the output of MSPL_GAN.

TABLE 7. Quantitative comparisons on testset of Shen *et al.* [7]. Best results are highlighted as bold.

	Helen				CelebA			
Method	PSNR(↑)	SSIM(↑)	d_{VGG}(↓)	LPIPS(↓)	PSNR(↑)	SSIM(↑)	d_{VGG}(↓)	LPIPS(↓)
Shen *et al.* [7]	25.58	0.861	91.06	0.1527	24.34	0.860	117.50	0.1832
Lu *et al.* [68]	20.25	0.705	241.93	0.1654	19.96	0.742	305.96	0.1688
Xia *et al.* [58]	26.13	0.886	55.97	0.1052	25.18	0.892	68.05	0.1199
Yasarla *et al.* [8]	**27.75**	**0.897**	86.87	0.1086	**26.62**	**0.908**	66.33	0.1401
MSPL_GAN	25.91	0.881	**47.80**	**0.0828**	24.91	0.885	**57.54**	**0.0962**

As shown in Table 6, our model significantly outperforms the previous state-of-the-arts in restoring individual classes of the face, especially for the inner parts of the face which contain small and important features of the face. These results show that our model effectively restores the facial image by reducing the class-imbalance problem compared to the previous methods.

2) Comparisons Using Shen *et al.* [7] Testset.

We conducted experiments on the testset provided by Shen *et al.* [7]. In Table 7, it can be noted that Yasarla *et al.* [8], and Xia and Chakrabarti [58] performed the best PSNR and SSIM. However, as can be seen in Fig. 6, the results obtained using the previous methods [7], [8], [58] are overly smoothed images, their models obtain better results in PSNR and SSIM compared to our model. As mentioned before, the

This article has been accepted for publication in a future issue of this journal, but has not been fully edited. Content may change prior to final publication. Citation information: DOI 10.1109/ACCESS.2020.3033890, IEEE Access

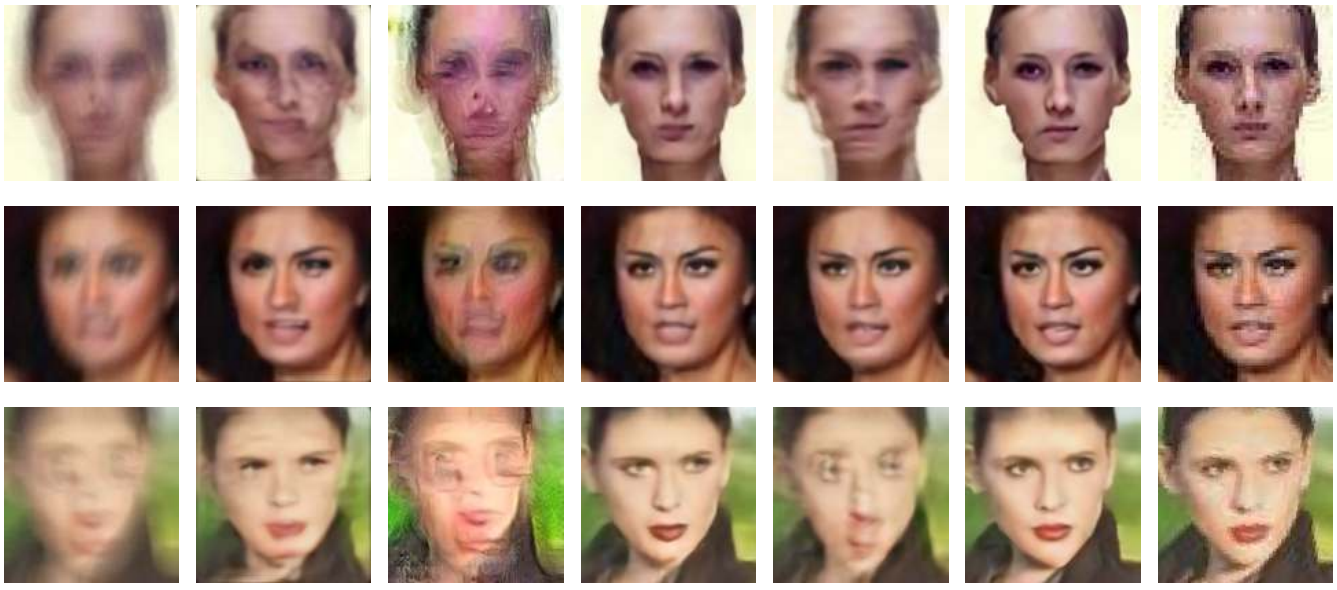

FIGURE 6. Qualitative comparison on Shen *et al.* [7] Testset.

TABLE 8. Quantitative comparisons on MSPL testsets. Best results are highlighted as bold.

	MSPL-Center											
	CelebA				CelebA-HQ				FFHQ			
Method	PSNR(↑)	SSIM(↑)	d_{VGG}(↓)	LPIPS(↓)	PSNR(↑)	SSIM(↑)	d_{VGG}(↓)	LPIPS(↓)	PSNR(↑)	SSIM(↑)	d_{VGG}(↓)	LPIPS(↓)
Shen *et al.* [7]	19.75	0.740	113.66	0.3007	19.95	0.755	267.41	0.2865	19.57	0.723	220.87	0.3417
Lu *et al.* [68]	17.93	0.617	123.35	0.2284	18.63	0.649	243.06	0.1902	18.26	0.630	177.00	0.2256
Zhang *et al.* [70]	20.40	0.744	117.68	0.3143	20.90	0.764	239.04	0.2952	20.64	0.743	170.41	0.3426
*Zhang *et al.* [70]	23.98	0.824	45.13	0.2412	24.84	0.844	83.36	0.2115	23.52	0.813	71.51	0.2866
Xia *et al.* [58]	25.03	0.873	39.58	0.1790	25.79	0.886	83.46	0.1608	24.66	0.859	57.66	0.2081
Yasarla *et al.* [8]	22.73	0.817	55.01	0.2132	23.02	0.827	102.97	0.1956	22.19	0.795	86.43	0.2506
MSPL_GAN	**28.07**	**0.921**	**18.19**	**0.1152**	**28.82**	**0.929**	**40.93**	**0.0968**	**27.36**	**0.908**	**25.39**	**0.1325**
	MSPL-Random											
	CelebA				CelebA-HQ				FFHQ			
Method	PSNR(↑)	SSIM(↑)	d_{VGG}(↓)	LPIPS(↓)	PSNR(↑)	SSIM(↑)	d_{VGG}(↓)	LPIPS(↓)	PSNR(↑)	SSIM(↑)	d_{VGG}(↓)	LPIPS(↓)
Shen *et al.* [7]	18.89	0.711	90.37	0.3310	19.18	0.729	157.49	0.3185	19.03	0.713	127.71	0.3356
Lu *et al.* [68]	17.41	0.631	46.05	0.2693	18.04	0.664	72.56	0.2297	17.94	0.654	65.06	0.2589
Zhang *et al.* [70]	19.36	0.702	86.772	0.3276	19.85	0.726	144.738	0.3109	19.77	0.715	122.070	0.3331
*Zhang *et al.* [70]	23.35	0.794	30.456	0.2535	24.09	0.817	54.063	0.2267	23.54	0.804	46.027	0.2546
Xia *et al.* [58]	23.66	0.849	30.94	0.2044	24.48	0.861	60.95	0.1940	23.95	0.855	44.62	0.2016
Yasarla *et al.* [8]	21.24	0.777	45.05	0.2448	21.46	0.789	72.56	0.2296	21.28	0.778	65.06	0.2407
MSPL_GAN	**28.95**	**0.936**	**11.41**	**0.1090**	**29.80**	**0.945**	**26.91**	**0.0938**	**29.22**	**0.941**	**15.44**	**0.0988**

problems of low-quality images in the Shen *et al.* [7] testset are noteworthy. The results in Fig. 6 show this problem more clearly. First, we can observe that not a few GT images have severe blocking artifacts (for example, see the last column in Fig. 6). Second, our model restores the sharp images that are even better than GT images. When comparing the GT images with our images, our results have sharper boundaries at the border of the facial components without blocking artifacts. These observations support that the existing Shen *et al.* [7] testset has a limitation in providing accurate deblurring evaluation.

On the other hand, the proposed MSPL w/o GAN and MSPL_GAN achieved the best performance in d_{VGG} and LPIPS with a huge margin, as listed in Table 7. The result of d_{VGG} indicates that our restored faces are similar to the GT images in terms of face identification. In addition, this shows that our model is the best model for higher vision task such as face recognition. LPIPS is the metric, which correlates better with human perceptual opinions [63]. The results of LPIPS show that the restored faces using our model are more visually plausible in terms of human vision.

3) Comparisons Using MSPL Testset.

In extended experiments on MSPL-Center and MSPL-Random testsets, we observed that our proposed method achieved the best performance both quantitatively and qualitatively. The quantitative results are listed in Table 8. The result values of PSNR, SSIM, d_{VGG}, and LPIPS indicate that

This article has been accepted for publication in a future issue of this journal, but has not been fully edited. Content may change prior to final publication. Citation information: DOI 10.1109/ACCESS.2020.3033890, IEEE Access

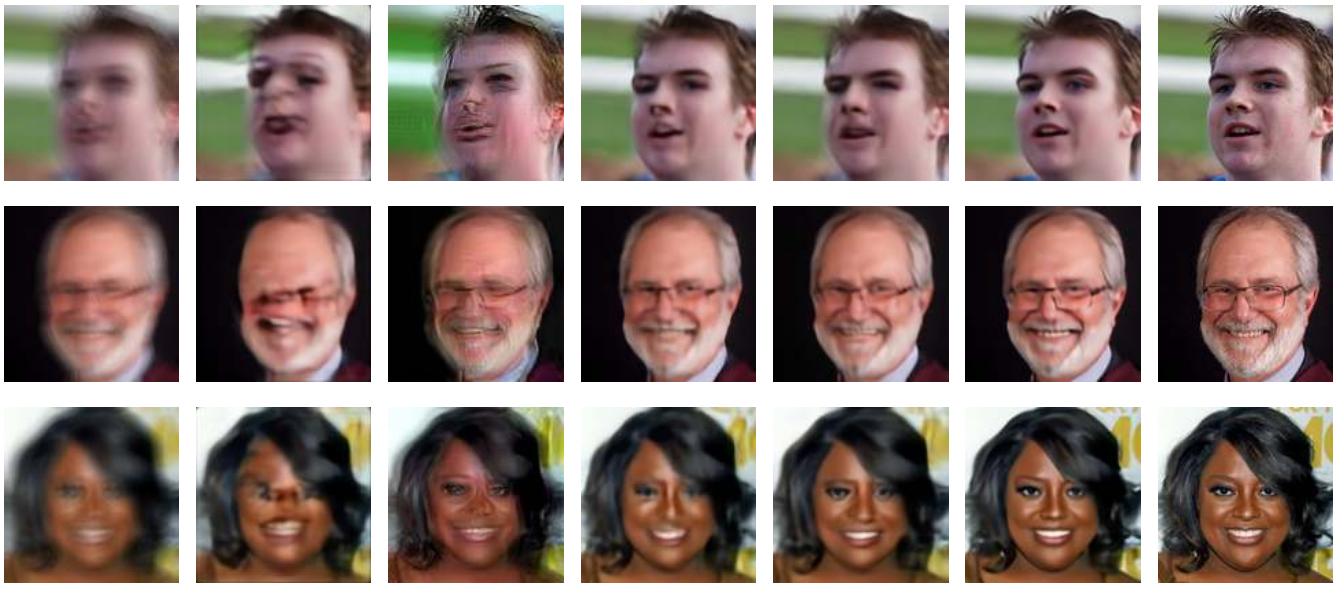

FIGURE 7. **Qualitative comparison on MSPL-Center Testset.**

FIGURE 8. **Qualitative comparison on MSPL-Random Testset.**

our framework significantly outperformed the existing methods. Additional visual results in Fig. 7 and Fig. 8 demonstrate that the proposed method restored sharper and more detailed face images than previous methods. In our experiments, we observed that the performance of Shen *et al.* [7] was sensitive to alignment and rotation. When a given blurred face image was aligned differently or rotated differently from the training face images, the restoration performance of Shen *et al.* [7] was severely degraded (refer to the second column images of Fig. 7). The results of Yasarla *et al.* [8] were visually plausible for all the test images. However, the restored small facial components (i.e., eyes, nose, mouth, and teeth) still lacked details and textures when the blurred artifacts were severe in the input image. Meanwhile, the proposed framework achieved superior performance compared to previous existing methods.

4) Real-world blurred Facial Images.

We conducted experiments on the twenty facial images distorted by real-world blur provided by [7], [71]. In the real-

This article has been accepted for publication in a future issue of this journal, but has not been fully edited. Content may change prior to final publication. Citation information: DOI 10.1109/ACCESS.2020.3033890, IEEE Access

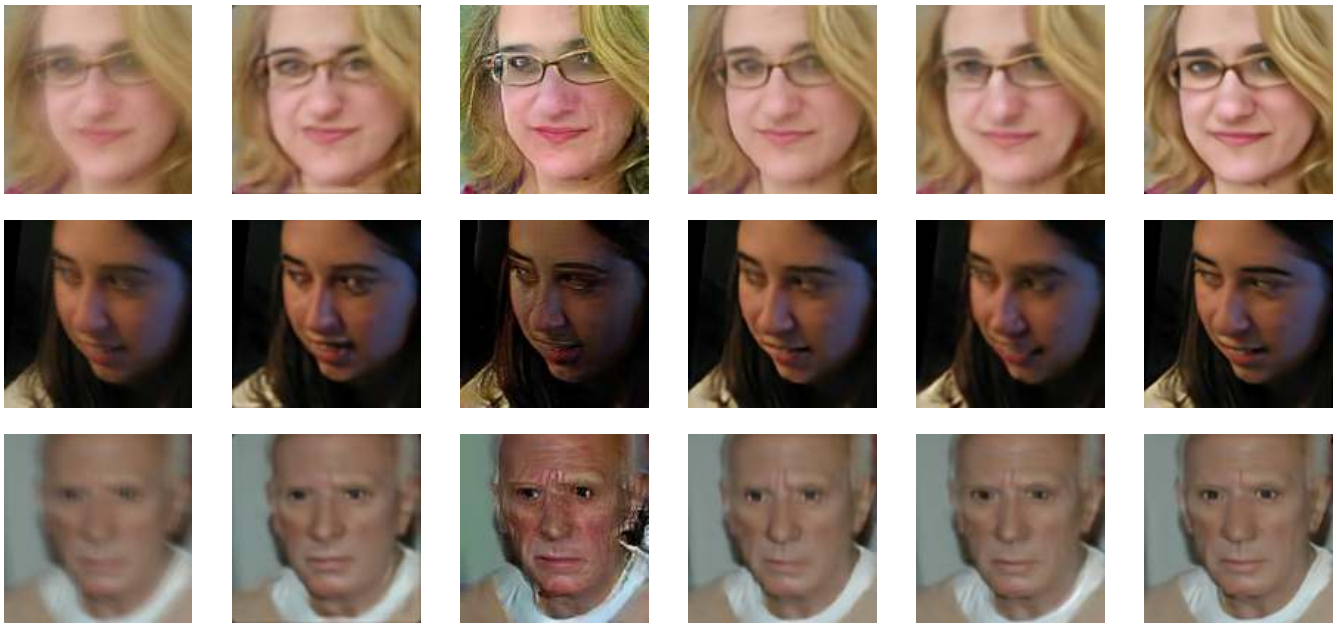

FIGURE 9. **Qualitative comparison on real-world blurred facial images.**

TABLE 9. **Comparison of average inference time and the number of model parameters.**

Method	Implementation	Inference time (S)	Parameters (M)
Shen *et al.* [7]	MATLAB(GPU)	0.05	14.8
Lu *et al.* [68]	Pytorch(GPU)	0.02	53.0
Xia *et al.* [58]	Tensorflow(GPU)	0.19	41.8
Yasarla *et al.* [8]	Pytorch(GPU)	0.16	14.4
Ours	Pytorch(GPU)	0.08	18.5

world, images are easily degraded with unknown complex factors such as the motion blur, lens distortion, sensor saturation, nonlinear transform functions, noise, and compression, in the camera pipeline [71]. However, all of these factors are not considered when generating the synthetically blurred images. Therefore, this experiment allows us to confirm the more practical performances of face deblurring methods that cannot be evaluated using the synthetically generated blur testsets. The comparative results of the sample images for the real-world blur are shown in Fig. 9. As can be seen in Fig. 9, the results of the proposed method show the most sharp and natural face images compared to other face deblurring methods. These results indicate that our proposed method has the capability of reconstructing the highest-quality images from the facial images with a real-world blur.

5) Inference Time and Model Parameters.

As shown in Table 9, we measured the inference time and the number of model parameters of the existing methods and the proposed model. The inference time is measured by averaging inference time of 10 images with a size of 128 $\times$ 128 on a single NVIDIA Titan Xp GPU.

TABLE 10. **Face detection and verification comparisons on the CelebA from the Shen *et al.* [7] testset.**

Method	Detection (%) (↑)	Acc (%) (↑)	EER (%) (↓)
GT of Shen *et al.* [7]	96.00	93.47	9.0909
Blurred images	77.40	77.05	18.7509
Shen *et al.* [7]	94.80	87.03	12.4398
Lu *et al.* [68]	89.03	80.56	17.4550
Xia *et al.* [58]	95.95	89.12	10.7587
Yasarla *et al.* [8]	94.49	87.84	11.9471
Ours	**96.55**	**89.59**	**10.0025**

When comparing the proposed model with the recent state-of-art model of Yasarla *et al.* [8], our model is slightly larger in number of parameters. However, it can be seen that our model is 2 times faster than Yasarla *et al.* [8]. This shows that the proposed method is more efficient than the two-stage deblurring method [8] consisting of segmentation and deblurring processes.

6) Face Detection and Verification.

Face detection and verification are important and practical tasks of localizing the faces and verifying an identity of each face in the image. One of the major goals of face deblurring is to increase accuracy in such high level tasks when the input image is blurry. For this reason, we compared the performances of face detection and verification using deblurred images on CelebA testset of Shen *et al.* [7].

For the detection test, we measured the success rate of the face detection using OpenFace toolbox [72]. As listed in Table 10, the success rates of the face detection for GT images, blurry images, and deblurred images using our model

are 96.00 %, 77.40 % and 96.55 %, respectively. It can be observed that our model achieved better performance than other methods, and even higher performance than the GT images of Shen *et al.* [7] testset.

We also measured the performances of the face verification on deblurred images. The CelebA testset of Shen *et al.* [7] contains 8000 blurry images synthesized with 100 GT images with different identities. From the original CelebA [60], we collected 200 additional images; 100 images of the same identities and 100 images of different identities with Shen *et al.* [7]. From this collected images, we generated the 8000 positive pairs and 8000 negative pairs. Each positive pair consists of a blurry image from the Shen *et al.* [7] testset, and a sharp image from the original CelebA [60]. They are different images of the same person. Each negative pair is also a set of a blurry image and a sharp image selected from the Shen *et al.* [7] testset and the original CelebA [60], respectively. Unlike the positive pair, their identities are different.

For the verification test, we use MobileNet [73] as a feature extractor trained with Arcface [74] loss and MS-Celeb-1M [75], which yields the 99.18 % accuracy on LFW benchmark [76]. To compare the verification performance, we measured the estimated mean accuracy (Acc) [76]. Equal error rate (EER) is another classical metric for face verification, which indicates the rate where both false acceptance rate and false rejection rate are equal. In general, the ideal EER value is 0, and the lower EER represents more accurate face verification results.

As demonstrated in Table 10, the proposed model achieves the best performance in Acc and EER. The verification Acc for the blurred image is 77.05 %, and the Acc for the deblurred images using our model is increased to 89.59 %. The EER for the original blurred image is 18.7509 %, while the EER for the deblurred image using our model is reduced to 10.0025 %. As shown in Table 10, our model achieves the lowest error rate compared to the conventional models. The results prove that our deblurring model is best suited for high-level tasks such as detection and verification compared to other methods.

V. CONCLUSIONS

In this study, we propose a multi-semantic progressive learning framework for facial image deblurring. Our framework employs an effective GAN-based architecture to restore the semantic structures of the face progressively without performing semantic segmentation. To evaluate the more practical and accurate performances of face deblurring methods, we have provided additional new testsets. Overall, the proposed method outperforms the existing methods both qualitatively and quantitatively. To the best of our knowledge, this is the first study on facial image deblurring using a semantic in progressive approach. We believe that our framework provides a potential approach for numerous other facial image restoration fields.

REFERENCES

[1] Y. Hacohen, E. Shechtman, and D. Lischinski, "Deblurring by example using dense correspondence," in *Proc. IEEE Int. Conf. Comput. Vis. (ICCV)*, Dec. 2013, pp. 2384–2391.

[2] J. Pan, Z. Hu, Z. Su, and M.-H. Yang, "Deblurring face images with exemplars," in *Proc. Eur. Conf. Comput. Vis. (ECCV)*. Springer, Sept. 2014, pp. 47–62.

[3] W. Ren, J. Yang, S. Deng, D. Wipf, X. Cao, and X. Tong, "Face Video Deblurring using 3D Facial Priors," in *Proc. IEEE Int. Conf. Comput. Vis. (ICCV)*, Oct. 2019, pp. 9388–9397.

[4] G. G. Chrysos and S. Zafeiriou, "Deep face deblurring," in *Proc. IEEE Conf. Comput. Vis. Pattern Recognit. Workshops (CVPRW)*, July 2017, pp. 69–78.

[5] G. G. Chrysos, P. Favaro, and S. Zafeiriou, "Motion deblurring of faces," *Int. J. Comput. Vis.*, vol. 127, no. 6-7, pp. 801–823, Mar. 2019.

[6] S. Lin, J. Zhang, J. Pan, Y. Liu, Y. Wang, J. Chen, and J. Ren, "Learning to Deblur Face Images via Sketch Synthesis," *Proc. AAAI Conf. Artif. Intell.*, vol. 34, pp. 11 523–11 530, Apr. 2020.

[7] Z. Shen, W.-S. Lai, T. Xu, J. Kautz, and M.-H. Yang, "Deep semantic face deblurring," in *Proc. IEEE Conf. Comput. Vis. Pattern Recognit. (CVPR)*, June 2018, pp. 8260–8269.

[8] R. Yasarla, F. Perazzi, and V. M. Patel, "Deblurring face images using uncertainty guided multi-stream semantic networks," *IEEE Trans. Image Process.*, Apr. 2020.

[9] Y. Chen, Y. Tai, X. Liu, C. Shen, and J. Yang, "Fsrnet: End-to-end learning face super-resolution with facial priors," in *Proc. IEEE Conf. Comput. Vis. Pattern Recognit. (CVPR)*, June 2018, pp. 2492–2501.

[10] I. Goodfellow, J. Pouget-Abadie, M. Mirza, B. Xu, D. Warde-Farley, S. Ozair, A. Courville, and Y. Bengio, "Generative adversarial nets," in *Adv. Neural Inf. Process. Syst. (NIPS)*, June 2014, pp. 2672–2680.

[11] T. Karras, T. Aila, S. Laine, and J. Lehtinen, "Progressive growing of gans for improved quality, stability, and variation," *arXiv preprint arXiv:1710.10196*, Oct. 2017.

[12] A. Karnewar and O. Wang, "MSG-GAN: Multi-Scale Gradients for Generative Adversarial Networks," in *Proc. IEEE Conf. Comput. Vis. Pattern Recognit. (CVPR)*, June 2020, pp. 7799–7808.

[13] R. Fergus, B. Singh, A. Hertzmann, S. T. Roweis, and W. T. Freeman, "Removing Camera Shake from a Single Photograph," in *ACM SIGGRAPH 2006 Papers*, ser. SIGGRAPH '06. New York, NY, USA: Association for Computing Machinery, July 2006, p. 787–794. [Online]. Available: https://doi.org/10.1145/1179352.1141956

[14] D. Krishnan, T. Tay, and R. Fergus, "Blind deconvolution using a normalized sparsity measure," in *Proc. IEEE Conf. Comput. Vis. Pattern Recognit. (CVPR)*. IEEE, June 2011, pp. 233–240.

[15] L. Xu, S. Zheng, and J. Jia, "Unnatural l0 sparse representation for natural image deblurring," in *Proc. IEEE Conf. Comput. Vis. Pattern Recognit. (CVPR)*, June 2013, pp. 1107–1114.

[16] W. Ren, X. Cao, J. Pan, X. Guo, W. Zuo, and M.-H. Yang, "Image deblurring via enhanced low-rank prior," *IEEE Trans. Image Process.*, vol. 25, no. 7, pp. 3426–3437, July 2016.

[17] T. Michaeli and M. Irani, "Blind deblurring using internal patch recurrence," in *Proc. Eur. Conf. Comput. Vis. (ECCV)*. Springer, Sept. 2014, pp. 783–798.

[18] L. Sun, S. Cho, J. Wang, and J. Hays, "Edge-based blur kernel estimation using patch priors," in *IEEE Int. Conf. Comput. Photography (ICCP)*, June 2013, pp. 1–8.

[19] J. Pan, D. Sun, H. Pfister, and M.-H. Yang, "Blind image deblurring using dark channel prior," in *Proc. IEEE Conf. Comput. Vis. Pattern Recognit.(CVPR)*, 2016, pp. 1628–1636.

[20] Y. Yan, W. Ren, Y. Guo, R. Wang, and X. Cao, "Image deblurring via extreme channels prior," in *Proc. IEEE Conf. Comput. Vis. Pattern Recognit. (CVPR)*, July 2017, pp. 4003–4011.

[21] Y. LeCun, Y. Bengio, and G. Hinton, "Deep learning," *Nature*, vol. 521, no. 7553, pp. 436–444, May 2015.

[22] J. Sun, W. Cao, Z. Xu, and J. Ponce, "Learning a convolutional neural network for non-uniform motion blur removal," in *Proc. IEEE Conf. Comput. Vis. Pattern Recognit. (CVPR)*, Oct. 2015, pp. 769–777.

[23] A. Chakrabarti, "A neural approach to blind motion deblurring," in *Proc. Eur. Conf. Comput. Vis. (ECCV)*. Springer, Sept. 2016, pp. 221–235.

[24] S. Nah, T. Hyun Kim, and K. Mu Lee, "Deep multi-scale convolutional neural network for dynamic scene deblurring," in *Proc. IEEE Conf. Comput. Vis. Pattern Recognit. (CVPR)*, July 2017, pp. 3883–3891.

[25] X. Tao, H. Gao, X. Shen, J. Wang, and J. Jia, "Scale-recurrent network for deep image deblurring," in *Proc. IEEE Conf. Comput. Vis. Pattern Recognit. (CVPR)*, Dec. 2018, pp. 8174–8182.

[26] O. Kupyn, V. Budzan, M. Mykhailych, D. Mishkin, and J. Matas, "DeblurGAN: Blind Motion Deblurring Using Conditional Adversarial Networks," in *Proc. IEEE Conf. Comput. Vis. Pattern Recognit. (CVPR)*, June 2018, pp. 8183–8192.

[27] B. Zhao, W. Li, and W. Gong, "Deep Pyramid Generative Adversarial Network With Local and Nonlocal Similarity Features for Natural Motion Image Deblurring," *IEEE Access*, vol. 7, no. Dec., pp. 185 893–185 907, 2019.

[28] Z. Zhao, B. Xiong, S. Gai, and L. Wang, "Improved Deep Multi-Patch Hierarchical Network With Nested Module for Dynamic Scene Deblurring," *IEEE Access*, Mar. 2020.

[29] K. Liu, C. Yeh, J. Chung, and C. Chang, "A Motion Deblur Method Based on Multi-Scale High Frequency Residual Image Learning," *IEEE Access*, Apr. 2020.

[30] Y. Blau and T. Michaeli, "The perception-distortion tradeoff," in *Proc. IEEE Conf. Comput. Vis. Pattern Recognit. (CVPR)*, June 2018, pp. 6228–6237.

[31] K. Grm, W. J. Scheirer, and V. Štruc, "Face hallucination using cascaded super-resolution and identity priors," *IEEE Trans. Image Process.*, vol. 29, no. 1, pp. 2150–2165, Oct. 2019.

[32] S. Cho and S. Lee, "Fast motion deblurring," in ACM SIGGRAPH Asia 2009 papers, Dec. 2009, pp. 1–8.

[33] L. Xu and J. Jia, "Two-phase kernel estimation for robust motion deblurring," in *Proc. Eur. Conf. Comput. Vis. (ECCV)*. Springer, Sept. 2010, pp. 157–170.

[34] D. Eigen, C. Puhrsch, and R. Fergus, "Depth map prediction from a single image using a multi-scale deep network," in *Adv. Neural Inf. Process. Syst. (NIPS)*, June 2014, pp. 2366–2374.

[35] A. Dosovitskiy, P. Fischer, E. Ilg, P. Hausser, C. Hazirbas, V. Golkov, P. Van Der Smagt, D. Cremers, and T. Brox, "Flownet: Learning optical flow with convolutional networks," in *Proc. IEEE Int. Conf. Comput. Vis. (ICCV)*, June 2015, pp. 2758–2766.

[36] D. Eigen and R. Fergus, "Predicting depth, surface normals and semantic labels with a common multi-scale convolutional architecture," in *Proc. IEEE Int. Conf. Comput. Vis. (ICCV)*, Dec. 2015, pp. 2650–2658.

[37] M. Mathieu, C. Couprie, and Y. LeCun, "Deep multi-scale video prediction beyond mean square error," *arXiv preprint arXiv:1511.05440*, Nov. 2015.

[38] E. L. Denton, S. Chintala, R. Fergus et al., "Deep generative image models using a laplacian pyramid of adversarial networks," in *Adv. Neural Inf. Process. Syst. (NIPS)*, June 2015, pp. 1486–1494.

[39] I. Durugkar, I. Gemp, and S. Mahadevan, "Generative multi-adversarial networks," *arXiv preprint arXiv:1611.01673*, Nov. 2016.

[40] H. Zhang, T. Xu, H. Li, S. Zhang, X. Wang, X. Huang, and D. N. Metaxas, "Stackgan: Text to photo-realistic image synthesis with stacked generative adversarial networks," in *Proc. IEEE Int. Conf. Comput. Vis. (ICCV)*.

[41] ——, "Stackgan++: Realistic image synthesis with stacked generative adversarial networks," *IEEE Trans. Pattern Anal. Mach. Intell.*, vol. 41, no. 8, pp. 1947–1962, July 2018.

[42] T. Karras, S. Laine, and T. Aila, "A style-based generator architecture for generative adversarial networks," in *Proc. IEEE Conf. Comput. Vis. Pattern Recognit. (CVPR)*, 2019, pp. 4401–4410.

[43] J. Yang, A. Kannan, D. Batra, and D. Parikh, "Lr-gan: Layered recursive generative adversarial networks for image generation," *arXiv preprint arXiv:1703.01560*, Mar. 2017.

[44] K. He, X. Zhang, S. Ren, and J. Sun, "Deep residual learning for image recognition," in *Proc. IEEE Conf. Comput. Vis. Pattern Recognit. (CVPR)*, June 2016, pp. 770–778.

[45] B. Lim, S. Son, H. Kim, S. Nah, and K. Mu Lee, "Enhanced deep residual networks for single image super-resolution," in *Proc. IEEE Conf. Comput. Vis. Pattern Recognit. Workshops (CVPRW)*, July 2017, pp. 136–144.

[46] X. Wang, K. Yu, S. Wu, J. Gu, Y. Liu, C. Dong, Y. Qiao, and C. Change Loy, "Esrgan: Enhanced super-resolution generative adversarial networks," in Proceedings of the European Conference on Computer Vision (ECCV), Oct. 2018, pp. 0–0.

[47] J. Hu, L. Shen, and G. Sun, "Squeeze-and-excitation networks," in *Proc. IEEE Conf. Comput. Vis. Pattern Recognit. (CVPR)*, June 2018, pp. 7132–7141.

[48] Y. Zhang, K. Li, K. Li, L. Wang, B. Zhong, and Y. Fu, "Image super-resolution using very deep residual channel attention networks," in Proceedings of the European Conference on Computer Vision (ECCV), Sept. 2018.

[49] T. Miyato, T. Kataoka, M. Koyama, and Y. Yoshida, "Spectral normalization for generative adversarial networks," *arXiv preprint arXiv:1802.05957*, Feb. 2018.

[50] J. Johnson, A. Alahi, and L. Fei-Fei, "Perceptual losses for real-time style transfer and super-resolution," in *Proc. Eur. Conf. Comput. Vis. (ECCV)*. Springer, Oct. 2016, pp. 694–711.

[51] K. Simonyan and A. Zisserman, "Very deep convolutional networks for large-scale image recognition," *arXiv preprint arXiv:1409.1556*, Sept. 2014.

[52] A. Mittal, R. Soundararajan, and A. C. Bovik, "Making a "completely blind" image quality analyzer," IEEE Signal Process. Lett., vol. 20, no. 3, pp. 209–212, Mar. 2012.

[53] A. Mittal, A. K. Moorthy, and A. C. Bovik, "No-reference image quality assessment in the spatial domain," *IEEE Trans. Image Process.*, vol. 21, no. 12, pp. 4695–4708, Aug. 2012.

[54] C. Ma, C.-Y. Yang, X. Yang, and M.-H. Yang, "Learning a no-reference quality metric for single-image super-resolution," *Comput. Vis. Image Understanding*, vol. 158, pp. 1–16, Dec. 2017.

[55] N. Venkatanath, D. Praneeth, M. C. Bh, S. S. Channappayya, and S. S. Medasani, "Blind image quality evaluation using perception based features," in *Nat. Conf. Commun. (NCC)*. IEEE, Apr. 2015, pp. 1–6.

[56] A. Ignatov, R. Timofte, T. Van Vu, T. Minh Luu, T. X Pham, C. Van Nguyen, Y. Kim, J.-S. Choi, M. Kim, J. Huang et al., "Pirm challenge on perceptual image enhancement on smartphones: Report," in *Proc. Eur. Conf. Comput. Vis. (ECCV)*, Oct. 2018, pp. 0–0.

[57] C.-H. Lee, Z. Liu, L. Wu, and P. Luo, "MaskGAN: Towards Diverse and Interactive Facial Image Manipulation," in *Proc. IEEE Conf. Comput. Vis. Pattern Recognit. (CVPR)*, June 2020.

[58] Z. Xia and A. Chakrabarti, "Training Image Estimators without Image Ground Truth," in *Adv. Neural Inf. Process. Syst. (NIPS)*, 2019, pp. 2436–2446.

[59] A. Kae, K. Sohn, H. Lee, and E. Learned-Miller, "Augmenting CRFs with Boltzmann machine shape priors for image labeling," in *Proc. IEEE Conf. Comput. Vis. Pattern Recognit. (CVPR)*, June 2013, pp. 2019–2026.

[60] Z. Liu, P. Luo, X. Wang, and X. Tang, "Deep Learning Face Attributes in the Wild," in *Proc. IEEE Int. Conf. Comput. Vis. (ICCV)*, December 2015.

[61] E. Agustsson and R. Timofte, "Ntire 2017 challenge on single image super-resolution: Dataset and study," in *Proc. IEEE Conf. Comput. Vis. Pattern Recognit. Workshops (CVPRW)*, July 2017, pp. 126–135.

[62] Y. Wang, L. Wang, J. Yang, W. An, and Y. Guo, "Flickr1024: A large-scale dataset for stereo image super-resolution," in *Proc. IEEE Int. Conf. Comput. Vis. Workshops (ICCVW)*, Oct. 2019, pp. 0–0.

[63] A. Lugmayr, M. Danelljan, and R. Timofte, "Ntire 2020 challenge on real-world image super-resolution: Methods and results," in *Proc. IEEE Conf. Comput. Vis. Pattern Recognit. (CVPR)*.

[64] A. Paszke, S. Gross, F. Massa, A. Lerer, J. Bradbury, G. Chanan, T. Killeen, Z. Lin, N. Gimelshein, L. Antiga et al., "Pytorch: An imperative style, high-performance deep learning library," pp. 8026–8037, June 2019.

[65] D. P. Kingma and J. Ba, "Adam: A method for stochastic optimization," *arXiv preprint arXiv:1412.6980*, Dec. 2014.

[66] Z. Wang, A. C. Bovik, H. R. Sheikh, and E. P. Simoncelli, "Image quality assessment: from error visibility to structural similarity," *IEEE Trans. Image Process.*, vol. 13, no. 4, pp. 600–612, Apr. 2004.

[67] O. M. Parkhi, A. Vedaldi, and A. Zisserman, "Deep Face Recognition," pp. 41.1–41.12, September 2015. [Online]. Available: https://dx.doi.org/10.5244/C.29.41

[68] B. Lu, J.-C. Chen, and R. Chellappa, "Unsupervised domain-specific deblurring via disentangled representations," in *Proc. IEEE Conf. Comput. Vis. Pattern Recognit. (CVPR)*, June. 2019, pp. 10 225–10 234.

[69] R. Zhang, P. Isola, A. A. Efros, E. Shechtman, and O. Wang, "The unreasonable effectiveness of deep features as a perceptual metric," in *Proc. IEEE Conf. Comput. Vis. Pattern Recognit. (CVPR)*, June 2018, pp. 586–595.

[70] H. Zhang, Y. Dai, H. Li, and P. Koniusz, "Deep Stacked Hierarchical Multi-patch Network for Image Deblurring," in *Proc. IEEE Conf. Comput. Vis. Pattern Recognit. (CVPR)*, June 2019, pp. 5978–5986.

[71] W. Lai, J. Huang, Z. Hu, N. Ahuja, and M. Yang, "A Comparative Study for Single Image Blind Deblurring," in *Proc. IEEE Conf. Comput. Vis. Pattern Recognit. (CVPR)*, June 2016.

[72] B. Amos, B. Ludwiczuk, and M. Satyanarayanan, "OpenFace: A general-purpose face recognition library with mobile applications," CMU-CS-16-118, CMU School of Computer Science, Tech. Rep., 2016.

[73] A. G. Howard, M. Zhu, B. Chen, D. Kalenichenko, W. Wang, T. Weyand, M. Andreetto, and H. Adam, "Mobilenets: Efficient convo-

lutional neural networks for mobile vision applications," *arXiv preprint arXiv:1704.04861*, 2017.

[74] J. Deng, J. Guo, N. Xue, and S. Zafeiriou, "Arcface: Additive angular margin loss for deep face recognition," in *Proc. IEEE Conf. Comput. Vis. Pattern Recognit. (CVPR)*, 2019, pp. 4690–4699.

[75] Y. Guo, L. Zhang, Y. Hu, X. He, and J. Gao, "Ms-celeb-1m: A dataset and benchmark for large-scale face recognition," in European conference on computer vision. Springer, 2016, pp. 87–102.

[76] G. B. Huang, M. Ramesh, T. Berg, and E. Learned-Miller, "Labeled faces in the wild: A database for studying face recognition in unconstrained environments," University of Massachusetts, Amherst, Tech. Rep. 07-49, October 2007.

TAE BOK LEE received the B.S. degree in Electrical and Computer Engineering in 2018, from Ajou University, Suwon, Korea. He is currently pursuing integrated M.S. and Ph.D. degree in Department of Artificial Intelligence at Ajou University, Suwon, Korea. His research interests include computer vision, deep learning and image restoration.

SOO HYUN JUNG received the B.S. degree in Electronic and Electrical Engineering in 2019, from Dongguk University, Seoul, Korea. She is currently pursuing the M.S. degree in Electrical and Computer Engineering at Ajou University, Suwon, Korea. Her research interests include computer vision, deep learning, image restoration and visual reasoning.

YONG SEOK HEO received the BS degree in Electrical Engineering in 2005, and the MS and the Ph.D. degrees in Electrical Engineering and Computer Science in 2007 and 2012, respectively, from Seoul National University, Korea. During 2012–2014, he was with Samsung Electronics, in the Digital Media and Communications R&D Center. Currently, he is with the Department of Electrical and Computer Engineering and the Department of Artificial Intelligence at Ajou University as an associate professor. His research interests include segmentation, stereo matching, 3D reconstruction, and computational photography.